Experimental Investigation of a High-Energy Density, High-Pressure Arc Plasma

EDWARD A. MARTIN
The University of Michigan, Ann Arbor, Michigan
(Received September 21, 1959)

The underwater spark is utilized to study the fundamental parameters of a plasma at 30 000°K and 10 000 atmos pressure. The 25-kv spark is obtained by underwater discharge of capacitors having a stored energy of 1800 joules, the inertia of the water providing the confinement necessary to develop high pressures. Phenomena relating to the initiating wire (exploded wire) are discussed. Kerr cell photographs show that spherical structures are formed around both electrodes under certain conditions. A possible explanation is postulated. A detailed energy balance and particle balance are carried out. The results show that the plasma has great capability to store energy in dissociation, excitation, and ionization without a corresponding increase in temperature. The plasma is 30% ionized and the total particle density is about 2×10^{27} per cubic meter. At this density the plasma radiates a blackbody spectrum. Pressures are obtained by calculation based on the rate of spark channel expansion and the shock properties of water. The plasma is found to have an internal pressure of the same order of magnitude as the external pressure because of interparticle Coulomb forces. Plasma conductivity calculated from equations of Gvosdover and Spitzer and Harm agree very well with the experimental value. The study is basically experimental, with the emphasis in interpretation being placed on reliability of the conclusions rather than on refined accuracy.

INTRODUCTION

THERE are two serious experimental obstacles which hinder the study of physical conditions within a high-pressure, high-temperature gas. Confinement of the gas to maintain its pressure requires thermal and mechanical properties of the chamber material which are beyond those presently available; and energy must be continually supplied to the gas at a high rate to replenish that lost by radiation. For these reasons, studies of steady state gases have been primarily concerned with temperatures not exceeding 10 000 °K and with pressures below 1000 atmos. If the studies are carried out on a transient basis, however, one can extend appreciably the pressure and temperature ranges to higher values. The underwater spark, produced by the rapid discharge of a capacitor across underwater electrodes, is an experimentally convenient means of producing and studying a highly ionized, high-pressure, high-temperature gas (plasma).

When a spark takes place under water, the heated spark plasma tends to expand. The mechanical inertia of the surrounding water resists this expansion, resulting in the development of high pressures. The objective, therefore, is to supply the maximum possible power to spark channel while the volume is still small. This calls for a maximum rate of current rise together with high spark resistance. The high pressures tend to increase spark resistance by reducing the degree of ionization and by reducing the mobility of the charged plasma particles.

The underwater spark has been used for many years as a spectroscopic light source. With a stored energy of several joules per discharge the radiant output has a continuum in the ultraviolet which is useful for absorption studies. The underwater spark may also find application as a photographic light source of high brilliance,[1] a subaqueous sound source,[2] or a pressure source. The emphasis in the present investigation, however, is to treat the underwater spark as a research tool for the study of high-energy plasmas. By its use information has been obtained concerning the physical conditions existing within a plasma at temperatures up to 30 000 °K and at pressures of the order of 10 000 atmos.

To establish the orders of magnitude involved, the final results will be briefly summarized. The underwater spark is produced by a 25-kv discharge from a 5.8 μf capacitor. At the moment of peak current, which is 85 000 amp, the spark plasma radiates a continuous spectrum corresponding to a black body at 29 900°K. The external pressure produced by the channel is 8300 atmos. The electrical power input is 390 megawatts. The total particle density within the plasma is about 2×10^{27} per cubic meter; and the plasma is 30% ionized. The plasma exhibits such a large capability to store energy in the form of dissociation, excitation, ionization, and kinetic energy of random motion of the constituent particles that most of the electrical energy input to the spark is initially stored within the channel. This energy is then relatively slowly dissipated (slow on the time scale of the spark processes) as mechanical work to generate a shock wave and as thermal radiation from the surface. The particle density in the channel is great enough so that the radiation emitted is more characteristic of a solid than a gas, and the importance of Coulomb interparticle forces makes the use of the ideal gas law invalid as an equation of state.

The actual measurement procedure consisted of determining the power input to the spark as a function of time by means of a discharge-circuit energy balance.

[1] H. C. Early and E. A. Martin, *Communication and Electronics* (American Institute of Electrical Engineers, New York, 1956), Vol. 22, p. 788.
[2] H. H. Rust and H. Drubba, Z. angew. Phys. **5**, 251 (1953).

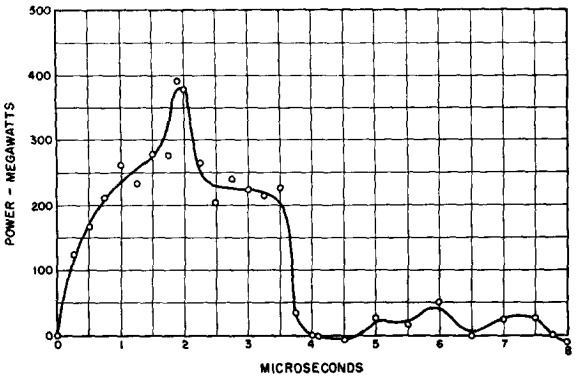

FIG. 1. Power delivered to the 25-kv underwater spark channel by the discharge circuit.

Subμsec Kerr cell camera photographs of the spark channel provided the channel size as a function of time. The channel pressure was determined from the rate of channel expansion and the shock characteristics of water. The channel temperature was determined by means of absolute measurements of the visible radiation. By use of these four fundamental spark parameters, a detailed energy balance for the plasma was carried out as a function of time. This energy balance involved the degrees of dissociation, excitation, and ionization within the channel. The conclusions which were reached are self-consistent as well as consistent with the work of others.

THE DISCHARGE CIRCUIT

The attainment of high pressure and high temperatures within the spark channel requires that the initial rate of current rise be maximized. To this end, the circuit was constructed to have as short leads as possible, and the leads consisted of closely spaced wide copper strips insulated to withstand the capacitor voltage used. The existence of high voltage and high current in the circuit required careful attention to electrical shielding and grounding; otherwise, large spurious signals induced in the triggering and measuring circuits invalidated the experimental data.

The electrical properties of the discharge circuit were as follows: The capacitors consisted of five 1-μf, 25-kv units connected in parallel and mounted inverted at the top of a metal cabinet. The electrical circuit was closed by means of a manually operated air gap, initiating the discharge through the underwater electrodes. On the microsecond time scale of the underwater spark, the 0.01 μsec breakdown time of the air gap could be treated as instantaneous closure of the circuit. The small energy dissipated in this air gap was taken into account in the circuit energy balance. A 15-gal covered water tank was positioned directly below the capacitors. A 3-in. diam window was located in the side of the tank so that photographs could be taken and light measurements made. Since the spark took place only $4\frac{3}{4}$ in. from the window, the shock wave accompanying the spark rendered the use of glass impractical. The material which was finally found to be successful was $\frac{5}{16}$ in. Plexiglas clamped between sheet rubber gaskets.

Current measurements were made by use of a folded ribbon shunt and recording oscilloscope (Tektronix 513-D and Polaroid camera). The shunt resistance and inductance were 0.00693 ohm and 2×10^{-11} henry. Maximum rate of change of current in the discharge circuit, 6×10^{10} amp/sec, would thus induce about one volt compared to the peak resistive voltage of 590 v.

The discharge circuit parameters were experimentally determined by use of conventional measurement equipment or by short-circuiting part of the discharge circuit and noting the current resulting from reduced voltage discharges. The methods used allowed for skin and proximity effects in the discharge circuit and for the effects of induced currents in the shielding cabinet. All values of circuit parameters were checked by approximate calculations based on physical dimensions. The effective series resistance and inductance of the energy storage capacitors were obtained by measurement. The results of the circuit measurements may be briefly summarized. The effective capacitance of the energy storage capacitors was 5.8 μf, the effective series inductance of the entire circuit was 0.26 μh, and the effective series resistance (including the contributions from the manual air gap and the current shunt) was 0.0422 ohm.

CIRCUIT ENERGY BALANCE

The circuit energy balance as a function of time was carried out by use of the measured spark current and the circuit parameters, the spark being treated as a passive circuit element. The current was integrated to obtain capacitor voltage. The derivative of current furnished the inductive voltage. By subtracting resistive and inductive powers from the capacitor power, the power to the spark was obtained (Fig. 1). These measurements and calculations were checked for accuracy by continuously accounting for all of the energy originally stored in the capacitor. This revealed that the errors in the circuit energy balance were of the order of one percent. A summary of these calculations is presented in Table I. The useful product of the energy balance is column 8 which gives the cumulative energy which has been supplied to the spark at any instant of time. It should be noted that half of the energy originally stored in the capacitors was transferred to the spark channel at 8 μsec. This high efficiency of energy transfer is jointly a result of high spark resistance caused by high plasma pressure and by low circuit inductance and resistance.

KERR CELL CAMERA

The Kerr cell camera photographs of the underwater spark yielded the rate of growth of the spark channel as well as much qualitative information. The Kerr cell utilized nitrobenzene as the active liquid. HN22 high

TABLE I. Circuit energy balance.

1 Time μsec	2 Current amp	3 Calculated capacitor voltage kv	4 Calculated instantaneous capacitor output power megawatts	5 Calculated instantaneous inductance input power megawatts	6 Calculated instantaneous resistive power megawatts	7 Instantaneous power to spark megawatts	8 Cumulative energy into spark joules	9 Error of circuit energy balance joules
0	0	25.00	0	0	0	0	0	0
¼	13 700	24.71	338	206	7.9	124	19	+4
½	31 000	23.76	736	527	40.5	168	54	+16
¾	46 600	22.08	1030	725	92.0	213	102	+18
1	58 700	19.84	1164	757	145	262	158	−13
1¼	70 100	17.05	1196	756	207	233	220	−9
1½	78 300	13.96	1094	558	258	278	286	−6
1¾	83 400	10.37	864	293	294	277	359	−10
1.9	85 000	8.19	696	0	305	391	413	+7
2	84 500	6.70	566	−113	301	378	451	+1
2¼	81 500	3.10	252	−292	280	264	528	−17
2½	76 900	−0.28	−21.6	−475	250	203	588	−13
2¾	69 000	−3.40	−234	−674	201	239	644	−17.5
3	57 300	−6.20	−356	−720	139	225	699	−33
3¼	44 700	−8.40	−376	−675	84.4	214	755	−24
3½	29 800	−10.00	−298	−464	37.5	128	809	−13.5
3¾	15 450	−11.00	−170	−214	10.1	34	835	−5.5
4	3 090	−11.40	−35.2	−39.8	4.0	½	838	−6
4½	−19 050	−10.60	+202	194	15.4	−7	837	−9
5	−34 600	−8.40	291	214	50.5	26	839	−3.5
5½	−42 900	−5.00	214	118	77.9	18	851	−6.5
6	−43 600	−1.30	56.6	−73.6	80.1	50	868	−9
6½	−38 400	+2.30	−88.4	−151	62.1	½	878	−7
7	−27 000	5.10	−138	−194	30.8	25	886	−12.5
7½	−10 420	6.75	−70.5	−102	4.6	27	899	−16
8	+7 820	6.81	+53.2	+62.5	2.6	−12	902	−16
						Magnitude of average error		11.7 joules

extinction Polaroids were used. All optical surfaces were adjustable so that not only extinction but also parallelism could be attained; this was found necessary in order to eliminate ghost images produced by multiple reflection. The cell was left open to the atmosphere so that changes in atmospheric pressure or temperature could not strain the windows. Contamination of the nitrobenzene through the small venting hole did not impair the operation of the cell. Evidently the pulse duration of ¼ μsec was not long enough to allow field-distorting space charges to accumulate within the liquid. The light-to-dark ratio was sufficiently high so that no photographic exposure could be detected when the spark was caused to take place with no voltage pulse applied to the Kerr cell electrodes. A 6-in. camera lens was used, the spark being in such a position as to result in an image on the film about 1.8 times actual size. The photographic speed of the entire optical system was about f/40.

The Kerr cell required a 7-kv pulse. This was obtained by use of a voltage-fed pulse network switched by means of a 5C22 hydrogen thyratron triggered by a 2D21 thyratron. The continuously adjustable delay trigger output of the oscilloscope was generally used, which gave delay times as short as one μsec after initiation of spark current flow. For shorter delays the 5C22 was triggered directly by the discharge circuit through an RC delay circuit.

SPHERICAL STRUCTURES

Initial work with the underwater spark was carried out at 4 to 10 kv using a storage capacitor of 11 μf. The sudden application of voltages of this magnitude to underwater electrodes which are approximately 1.5 cm apart does not result in immediate breakdown. There is a time lag of random duration during which a current of about one amp flows. At the lower capacitor voltages the breakdown lag may be several millisec. When the voltage is increased, the duration may be only 10 or 100 μsec. Photographs taken when breakdown finally does occur reveal spherical structures on the electrodes (Fig. 2). These structures have interesting properties. The sphere on the positive electrode is always larger. Surface textures vary from cloudy to glossy smooth. The spheres have not been observed for water temperatures above 15°C, but they grow quite readily at 10°C. Occasionally breakdown failed to occur at the lower voltages because the capacitor charge was depleted by the prebreakdown current. Even in this case the spheres were formed, a fact which was established by photographing them with an auxiliary flash light source. Under this condition, there was no detectable mechanical disturbance in the water, indicating that the spheres did not represent an appreciable change in water density. It is noteworthy that these spheres were consistent in their uniformly spherical structure, because the original electric field between the parallel rod electrodes was far

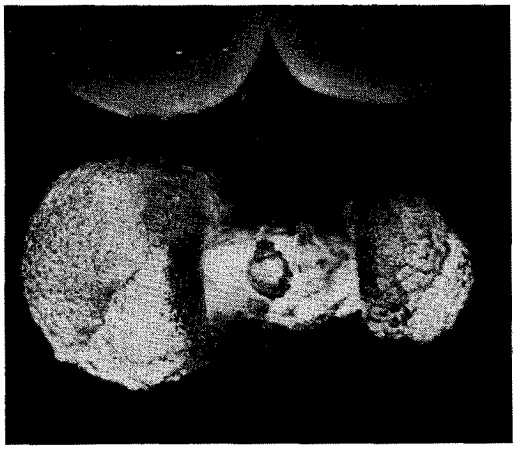

FIG. 2. Kerr cell photograph of a 6-kv underwater spark 10 μsec after breakdown. Left electrode positive.

from spherically symmetric. If a dielectric barrier was inserted between the electrodes to delay breakdown, the spheres grew very large, and while doing so they refused to contact a solid surface. The breakdown path always appeared to terminate at the centers of the spheres. In lieu of a better hypothesis, these spheres may possibly be regions of spontaneous electric polarization somewhat analogous to the magnetic domains in a ferromagnetic material. The surfaces of the spheres would then become visible because of an abrupt change in the dielectric constant of the water.

STREAMER BREAKDOWN

When the capacitors were charged to voltages of the order of 20 kv or more, breakdown took place so rapidly that the spheres did not form. The breakdown sequence resembled that which occurs in gases. One or both electrodes originated streamers. When a conducting path was established, the unsuccessful streamers became dormant, and their presence was revealed in the photographs by the light from the main discharge channel. The breakdown process required times of the order of several microseconds for voltages of the order of 20 kv.

INITIATING WIRE

The random duration of the prebreakdown period and the irregular, unpredictable path of the spark made correlation of data taken on different sparks very difficult. Also, the spheres, when present, tended to mask the channel geometry. These difficulties were all circumvented by initiating the spark with a fine wire between the electrodes. The resulting uniform, straight, circular cylinder, free of spheres, enabled the association of a definite and measurable geometry with the spark channel. In addition, the sparks became quite reproducible from one to the next. A large number of Kerr cell photographs and current oscillograms were taken to check reproducibility. Excellent consistency of the data justified the use of instantaneous measurements on successive sparks at increasingly later delay times as a means of obtaining the spark behavior as a function of time.

It was established that the metal of the initiating wire played no significant part in the plasma phenomena of the spark channel. Even though the atoms of the initiating wire were more highly ionized than the other particle components of the plasma, they neither contributed an appreciable number of particles nor stored an appreciable amount of energy. When larger size initiating wires were used at low voltages, a dip in the current shown by the current oscillogram revealed the moment at which the wire vaporized. For 3-mil copper wire at 6 kv, the vaporization time was about one μsec. However, for the spark measurements described in this paper, one-mil tungsten wire was used. In this case, the vaporization took place essentially instantaneously on the microsecond time scale of the spark.

It has been predicted on the basis of similarity that a spark channel in a gas under very high pressure should consist of a very fine filament. Such a channel, because of lateral instability, should continually be whipping about within the luminous column, successively exciting and ionizing small volume elements of the plasma and then moving on and leaving those elements to radiate the stored energy until the next lateral trip. It is not necessary to postulate that particles would have to attain a lateral velocity corresponding to the velocity of the filamentary channel, since the channel is merely a path of high ionization. This path could move at very high lateral velocities, too high to be revealed by a $\frac{1}{4}$-μsec photographic exposure. Various attempts were made to cause the postulated fine channel to reveal itself. The spark was initiated adjacent to a transparent material (plastic, mica, or glass) and then photographed through the resulting "window" before the material was destroyed, in order to see into the luminous column. Also, initiating wires were bent into hairpin shapes, or two underwater sparks were initiated parallel to each other, in an effort to make the mutual magnetic fields drive the fine channel out of the luminous column. Among the large number of Kerr cell pictures which were made, not one showed any evidence of the predicted fine filamentary channel.

STRIATIONS

Photographs of underwater sparks initiated by a relatively large diameter wire showed transverse striations during the early stages of spark development. They were occasionally very clear and sharply delineated. The spacing was a function of the initiating wire diameter but was relatively unaffected by changes in wire material. These striations were originated by unduloids, the succession of droplets which is formed when a wire is rapidly melted by an electric current. The unduloids are formed by the self-magnetic field of the wire acting on the current carried by the wire, the so-called pinch

effect. This effect, if acting alone, would constrict the wire at random intervals. The high degree of regularity of the unduloids, and hence of the observed striations, may be explained by considering the instability of a liquid cylinder caused by surface tension. The surface tension tends to cause the liquid cylinder to break up into uniformly spaced droplets, the spacing being dependent on the diameter of the wire. The spacing may be predicted on the basis of the work of Lord Rayleigh.[3] Surface tension provides the initial small regularly spaced constrictions in the wire cross section which are then amplified by the relatively much greater magnetic pinch forces. Therefore, at some stage of the vaporizing process, the initiating wire must consist of a succession of metallic droplets separated by short arcs in the metal vapor. The spacings of the striations observed on the Kerr cell photographs of the underwater spark were compared with the predicted values based on Rayleigh's work. The spacings were found to be one-half and one-fourth (but not one-third) the predicted values. This indicates that secondary and tertiary unduloids are formed.[4] In the case of a one-mil tungsten wire vaporized at 25 kv, the striations are not in evidence. Either they are unresolved in the photographs or are incompletely formed because of the short duration of the liquid phase.

CHANNEL GROWTH

The size of the channel of the underwater spark, a consistently uniform circular cylinder, may be scaled from the Kerr cell photographs. When this is done for successively later times in the spark cycle, a growth curve is obtained. For the 25-kv, 5.8-μf spark studied in this work, the diameter of the channel in millimeters was

$$D=1.8t^{0.52}, \tag{1}$$

where t is the time in μsec after current initiation. The length of the spark was 1.5 cm, determined by electrode separation. In other similar spark sequences at different values of voltage and storage capacitance, the exponent of t was always found to be close to one-half.

SPARK CHANNEL PRESSURE

The rapid transfer of a large amount of energy into the small volume of the spark channel raises its temperature and tends to make it expand. The enveloping medium opposes this expansion, the amount of opposition being dependent on the medium density and relatively independent of hydrostatic pressure. For this reason, sparks in liquids develop high transient pressures which result in production of shock waves. The shock wave is made evident by the loud metallic report which is heard when the pressure pulse reaches the walls of the water tank.

Consideration was given to the problem of measuring the pressures in the vicinity of the underwater spark. An electromechanical device is not feasible. A response time of less than one μsec, a pressure range up to 50 000 atmos or so, very small size, extreme ruggedness, and insensitivity to rapidly varying electric and magnetic fields are characteristics which are not presently available in any transducer. Since the underwater spark will punch slugs from sheet metal, a rough index of the pressure range was established by calculating the static pressures necessary to shear a corresponding amount of metal. A second approximate measurement of the pressures in the water adjacent to the spark channel was made by measuring the amount of compression of the water. Compression modifies the index of refraction of the water, and hence an optical measurement of the change of index is sufficient to establish the pressure. This measurement indicated pressures in the range 2500 to 5000 atmos, but the accuracy was not suitable for present purposes. Further attempts to measure pressure based on determining the amount of adiabatic compression of small bubbles of hydrogen located close to the spark were not successful.

Pressures adjacent to the surface of the underwater spark may, however, be obtained by calculation based on rate of channel expansion. These pressures depend only on the hydrodynamic properties of water and on the rate of expansion of the cylindrical spark channel, provided that negligible water is inducted into the spark channel through the channel wall. As a result of the channel particle balance calculations soon to be described, it was established that the amount of water consumed at the channel wall was sufficiently small so that the pressure calculations were not rendered inaccurate. For example, at the time of current maximum the measured rate of channel expansion was 348 m/sec. Induction of water through the channel wall accounted for a wall velocity of only 10 m/sec.

Explicit calculation of the pressures produced at an arbitrary point in the water surrounding the expanding cylinder, whether formulated in the Euler or the Lagrange form, is difficult because of the high degree of nonlinearity. If, however, one is satisfied with a partial solution, calculations suitable for present requirements may be obtained. The procedure involves using the Rankine-Hugonoit shock wave relations in differential rather than in incremental form, yielding the pressure and pressure gradient at the surface of the expanding cylinder. One does not obtain information concerning the pressure distribution throughout the entire compressed region surrounding the cylinder. The solution obtained may be treated as the two inner boundary conditions for the more complete pressure calculation. The details of the pressure calculation will not be presented here; only the resulting equations will be given. The shock characteristics of water are taken to be given by

$$P=A(\rho/\rho_0)^7-B, \tag{2}$$

[3] Lord Rayleigh, Proc. London Math. Soc. **10**, 4 (1878).
[4] W. Kleen, Ann. Physik **403**, 579 (1931).

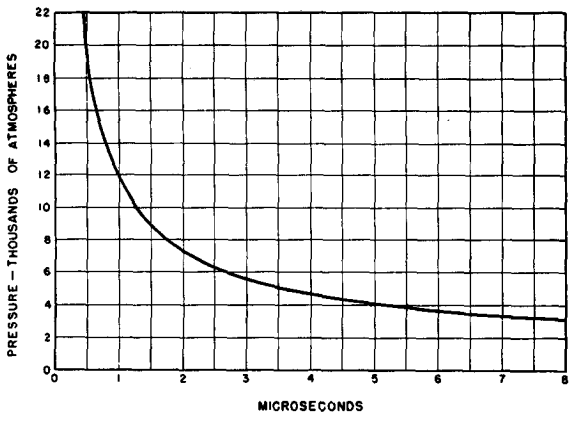

FIG. 3. Calculated pressure developed at the surface of a 25-kv underwater spark channel.

where P is pressure in atmos, ρ is the density at pressure P, ρ_0 is the normal density, and A and B are constants, equal to about 3000 atmos but differing by 1 atmos. Further, the separable-energy character of water is utilized so that only the relations concerning conservation of mass and momentum need be used. One may omit the small refinement of the solution resulting from consideration of the conservation of energy. The equations which result, giving the pressure and pressure gradient on the expanding cylinder surface, are

$$(P+B)^{3/7}=\left(\frac{3\rho_0^{1/2}}{7^{1/2}A^{1/14}}\right)U+B^{3/7}, \tag{3}$$

$$\frac{dP}{dr}=\frac{-(\rho_0)^{1/2}(dP/dt)}{7^{1/2}A^{1/14}(P+B)^{3/7}}-\frac{7(P+B)}{3r}+\frac{7(P+B)^{4/7}B^{3/7}}{3r}, \tag{4}$$

where U is the velocity of the cylinder wall (m/sec), r is the cylinder radius (meters), t is the time (sec), P is the pressure at the cylinder surface (newtons/meter^2), and ρ_0, A, and B are from Eq. (2) (MKS units). The value of dP/dt in Eq. (4) is obtained by differentiation of Eq. (3).

A plot of the pressure on the surface of the 25-kv underwater spark as a function of time is given in Fig. 3. The pressure curve has an infinite value at zero time because the exponent of the expansion relation, Eq. (1), is less than unity. The accuracy of measurement of spark diameters at times less than $\frac{1}{2}$ μsec was critically dependent on timing of the Kerr cell camera, and also the photographs have a finite exposure interval of $\frac{1}{4}$ μsec. Therefore, the expansion curve should not be considered valid during this early interval. The pressure curve should be considered as starting at zero initially and rapidly rising to a pressure of the order of 20 000 atmos in about $\frac{1}{2}$ μsec. The pressures given in Fig. 3 agree well with those obtained by measuring the change in optical index of the water, and are of the same order as the static pressures necessary to punch slugs from sheet metal.

MEASUREMENT OF TEMPERATURE

The underwater spark at high power levels emits a bluish-white flash of light. This light furnishes a means of measuring the temperature of the spark as a function of time. In general, the light emitted by a gas discharge will consist of spectral lines, recombination continua, and electron acceleration radiation (bremsstrahlung). For practical purposes, the light from a low pressure gas discharge below $\frac{1}{10}$ atmos is a pure line spectrum characteristic of the gas. As gas pressures are increased through the range from about $\frac{1}{10}$ atmos to several hundred atmos, the spectral lines broaden as a result of Doppler effect, collisional damping, Stark effect, and Zeeman splitting in the randomly varying local magnetic fields. Also, the recombination continuum becomes appreciable because of an increasing amount of volume recombination. As an example, hydrogen at approximately 30 atmos emits a continuous spectrum. The distribution of spectral intensity within the continuum, however, follows no simple mathematical law. Temperatures in many types of discharge may be determined by measuring the amount of spectral line broadening, the relative intensity of spectral lines, or the distribution of intensity in spectral bands. Such temperatures are not necessarily the temperatures corresponding to the average random thermal energy of any particular type of particle in the discharge. In general, unless there is thermal equilibrium among the various particle types, temperatures obtained by such measurements cannot be interpreted as temperature in the usual sense. Measurements carried out by two different methods will generally yield widely differing results.

As the gas pressure of an electrical discharge is progressively increased above approximately 200 atmos, the irregularities in the continuous spectrum which are caused by spectral lines or groups of spectral lines become submerged in the continuum. This continuum is produced partly by electron-ion recombination. However, at very high particle densities approaching the order of magnitude encountered in solid materials, the major contribution to the continuum is from electron acceleration radiation. The constituent plasma particles lose their individual spectral character. The plasma radiates a spectrum more characteristic of a solid than a gas. If certain conditions are fulfilled, the plasma should be expected to radiate a continuum having the spectral distribution of a black body. The measurements made during this investigation indicate that a high power underwater spark does radiate a blackbody spectrum.

There are two requirements which must be met in order for the continuum to have a blackbody distribution. First, all particle types within the plasma must be

in thermal equilibrium. This condition is approached when the freedom with which energy may be exchanged between different particle types is large enough so that the electrical input power to the plasma, which is primarily delivered to the electrons only, is transmitted to the other classes of particle types with only a small temperature difference being necessary. The freedom of energy transfer between the electrons and other particle types is measured by an accommodation time constant, which is determined by the rate of energy transfer through the mechanisms of elastic collisions, inelastic (dissociating, exciting, and ionizing) collisions, and radiant transfer. The over-all time constant (when all three mechanisms are operative) will of course always be shorter than the time constant for any one mechanism of transfer alone. A calculation on the basis of only one mechanism will give an upper limit to the true time constant. An accommodation time constant for the 25-kv spark being treated here, calculated on the basis of only elastic collisions between the electrons and ions of the plasma, gives a value of the order of 10^{-10} sec. The factors which enter into this calculation are the spark plasma temperature and particle densities. Thus, on the microsecond time scale of the underwater spark, the constituent particle types of the plasma may be considered to be in thermal equilibrium.

The second requirement for blackbody radiation is that the particle density must be great enough to render the plasma opaque to radiation which is in the spectral region of interest. From the viewpoint of photons, the mean free path of a photon must be small compared to the dimensions of the plasma. If this condition is satisfied, then a quantum which originates within the volume of the plasma is absorbed and re-emitted many times before escaping from the surface. When all particles with which the photon interacts have the same temperature, the situation is analogous to the absorption and re-emission of radiation within a blackbody enclosure at a uniform internal surface temperature. The plasma of the underwater spark is highly opaque. All Kerr cell photographs have failed to define any detail within the plasma volume. Also, for various reasons, the spark has been allowed to engulf a solid object during the course of its expansion. In the resulting Kerr cell photographs, the image of the object is sharply terminated at the channel surface. This evidence of opacity in the visible spectrum is the basis for concluding that the plasma has a very great absorption coefficient for radiation in the wavelength range in which the temperature measurements were made.

The spectrum of the light from the underwater spark was obtained by means of a quartz spectrograph. The spectral range covered was 3400 to 6900 A, and the exposures were time integrated over the entire spark history. Line structure could not be detected in the continuum. No attempt was made to determine spectral intensity as a function of wavelength because of the time-integrated nature of the exposures.

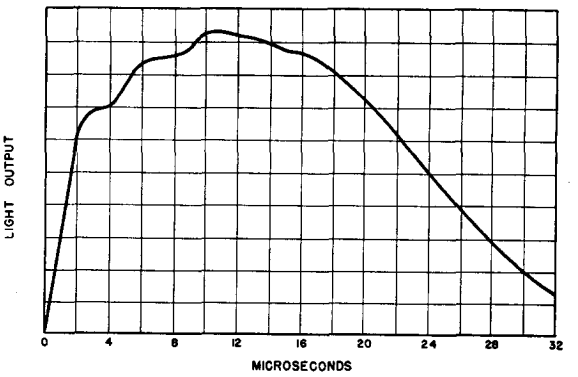

FIG. 4. Oscillogram of light output at 4190 A from the 25-kv underwater spark.

A conventional method of measuring the temperature of a body emitting a blackbody spectrum is to measure the relative spectral intensity at two wavelengths. However, when the temperatures are in the range of 30 000 °K or above, the method is of low accuracy if the measurements are made in the visible region of the spectrum. The visible region falls at wavelengths well beyond the maximum of the blackbody curve plotted on a wavelength scale, so that the ratio of the two measured intensities is a very insensitive function of the temperature. Therefore the temperature of the underwater spark was measured by determining the absolute intensity at a single wavelength. As a check, two completely independent measurements were made, one at the red end of the spectrum, and one at the blue end. Interference filters were used to isolate a known narrow spectral band, and vacuum phototubes were used. The phototube circuit for each measurement was enclosed in a shielding aluminum container together with the battery. The load resistor was made smaller than is typical in order to reduce the circuit time constant. Thorough checks were carried out to insure that the circuit frequency response and linearity were suitable, and that stray pickup and gas amplification were not present in sufficient amount to affect the measurements. The phototubes were calibrated against a tungsten ribbon standard lamp, which in turn had been calibrated by the use of optical pyrometers.

An oscillogram of the light output at 4190 A is shown in Fig. 4. An immediately evident significant fact is that the light output persists for about 30 μsec, whereas almost all of the electrical energy input is delivered to the spark in 4 μsec. This is evidence that the major amount of energy to the spark is stored within the plasma, this energy then being relatively slowly dissipated as the spark channel expands and cools. The light output oscillograms are shaped by the combined effects of channel expansion and decreasing temperature. As a result, oscillograms taken at the red end of the spectrum show the light output reaching a maximum slightly later than the light output at the blue end, but the total duration is approximately the same in both cases.

Utilizing the known sensitivity of the phototubes, the passband characteristics of the interference filters, the geometry of the measurements, the known size of the spark as obtained from the Kerr cell photographs, and the light output oscillograms, one may calculate the channel temperature as a function of time. In view of the opaque nature of the plasma, the resulting temperatures are the surface temperatures. In the calculations, the spark channel was taken to be a diffuse radiator inasmuch as the apparent brightness of the spark channel, as seen in the Kerr cell photographs, is uniform across the cross section even though the channel is a figure of revolution. The results of the two independent temperature measurements are presented in Fig. 5. Agreement is very good, tending to confirm the conclusion that the spark radiates as a black body.

In other temperature measurements which were made during the course of this study, the temperature measured at the red end of the spectrum has consistently been slightly lower than that obtained from the blue measurement. There are two possible causes for this discrepancy. If the spark channel surface has an emissivity less than unity, even though it may be independent of wavelength, then the true channel temperature would be greater than either of the measured values, and the blue measurement would give the higher value. The second possible cause is that the plasma absorption coefficient for red radiation may be somewhat greater than that for blue radiation.[5] If this is the case, the blue radiation will come from deeper layers within the spark channel where the temperature is somewhat higher.

The internal temperatures in the spark plasma are undoubtedly higher than the surface temperatures obtained from the preceding measurements. However, several considerations lead to the conclusion that these temperatures are not higher by a great factor. The first consideration is based on the apparent absence of a fine filamentary current-carrying channel within the luminous column of the spark. In addition, small calculated pinch pressures as compared to the total plasma pressure lead to the conclusion that the current density is substantially uniform across the spark cross section. Since most of the electrical energy supplied to the spark is stored in the plasma, any small volume unit will receive and store about the same amount of energy as any other volume unit, and thus will attain about the same temperature. There is no reason to require that there be an appreciable thermal gradient within the plasma in order to carry energy to the channel walls. The thermal conductivity of the plasma, to be calculated later, is low enough so that it would require a central temperature of about 3 million degrees in order to transmit to the channel walls the amount of power necessary to convert liquid water to channel plasma. Ion recombination on the channel wall will be shown to be more than adequate to supply this amount of power. The major power loss from the spark is that used in generating the shock wave. If all elemental volumes of the spark plasma expand uniformly, then this major energy loss is supplied without the necessity of a large thermal gradient to transport energy from the central regions of the channel to the spark environment. Further evidence that the spark does not have a central hot core is the inability of the ratio of channel cross-sectional area to lateral area to affect such spark parameters as light output, intrinsic brightness, peak current, and current damping. Photographs, light measurements, and current oscillograms were made with the underwater spark flattened between closely spaced surfaces. In spite of the consequent increase in the ratio of surface area to volume, the major parameters were not significantly altered. This behavior could not be expected if the central temperature were as much as an order of magnitude greater than the surface temperature. Finally, for the purposes of the energy balance to be described next, the central temperature is not of critical concern, since its value does not affect appreciably the energy balance. The density of energy storage in the spark plasma was found to be almost directly proportional to pressure and almost independent of temperature up to temperatures as high as 200 000°K.

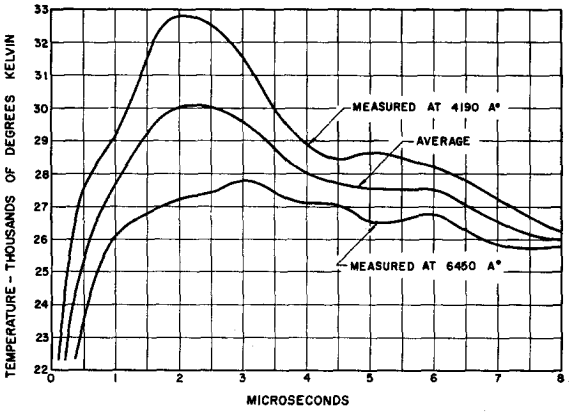

FIG. 5. Temperature of the underwater spark as determined by two independent measurements at two wavelengths. Note depressed zero.

[5] A star at 29 000°K should have a greater absorption coefficient for red light than for blue light. See L. H. Aller, *Astrophysics, the Atmospheres of the Sun and Stars* (Ronald Press Company, New York, 1953), p. 186.

THE SPARK ENERGY BALANCE

The preceding work has made available the spark channel size, the electrical input energy, the pressure, and the temperature as functions of time. These four parameters are the basis for a spark channel energy balance. The procedure will be concisely summarized. One begins with the total electrical energy which has been supplied to the spark by the discharge circuit previous to a selected instant of time. From this, one subtracts the total energy which has been lost from the channel by radiation, mechanical work, and thermal

conduction. Energy utilized at the channel wall to vaporize, dissociate, excite, and ionize incoming water should not be subtracted, since this energy is retained within the channel. The result obtained by this procedure is the energy actually resident within the channel at the selected instant of time.

The second part of the energy balance consists of employing the pressure, the temperature, the Saha and Boltzmann equations, and a plasma equation of state to obtain the plasma energy stored in the form of particle kinetic energy, dissociation, excitation, and ionization. The procedure may be termed a particle balance. The resulting plasma energy density multiplied by the spark channel volume yields the total energy stored in the spark channel. This result should agree with the channel energy obtained by the first method. The two procedures just described were used to calculate the stored energy as a function of time for the first eight μsec after initiation of current through the spark. These first eight μsec constitute the most interesting period of the spark history.

As suggested above, energy may be removed from the spark channel by radiation, by mechanical work to generate the shock wave, and by thermal conduction to the surrounding water. The radiant power output may be calculated using the Stephan Boltzmann law and the spark channel dimensions. The mechanical power output may be computed as the product of channel external pressure, wall velocity, and wall area. The power loss caused by thermal conduction is difficult to compute since the problem involves transient heat flow in which the dimensions of the hot body are changing and the hot surface is continually absorbing the adjacent water. Approximate calculations lead to a value of about 2 megawatts, which is small compared to the other two losses. Also, the heat transferred to the hottest water adjacent to the channel is reintroduced into the channel when this water is subsequently inducted. The thermal conduction loss will therefore be neglected. Calculated power losses at various moments due to radiation and mechanical work are given in Table II. Integrals of these losses furnish the total energies lost. These losses may be subtracted from the discharge circuit input energy to obtain the energy stored in the spark channel. The results are given in column 10 of Table II, and are plotted as Curve A in Fig. 6.

PARTICLE BALANCE

The second part of the energy balance requires that the number density of the various particle types in the spark plasma be determined. In general, one could write a complete set of particle balance equations involving as variables the number densities of all types of particles which could conceivably be found to exist in the plasma. This would involve all possible atom types in a wide range of conditions of association, excitation, and ionization. These particle balance equations,

TABLE II. Spark energy balance.

1 Time μsec	2 Channel diameter meters ($\times 10^{-3}$)	3 Channel volume cubic meters ($\times 10^{-6}$)	4 Channel wall velocity meters/sec	5 Calculated external pressure atmos	6 Shock wave power megawatts	7 Shock wave energy joules	8 Radiant power megawatts	9 Radiant energy joules	10 Channel energy (Curve A, Fig. 6) joules
0	0	0	∞	∞	∞	...	0	0	0
$\frac{1}{4}$	0.813	7.8	913	32 300	112.6	27.5	0.346	0.075	−8.6
$\frac{1}{2}$	1.25	18.4	657	19 400	75.0	44.5	1.41	0.300	+9.6
$\frac{3}{4}$	1.55	28.3	541	14 200	56.1	65.6	2.10	0.714	35.7
1	1.80	38.1	471	11 600	46.2	78.4	2.84	1.32	78.5
$1\frac{1}{4}$	2.02	48.0	423	9960	40.1	89.2	3.56	2.12	128.7
$1\frac{1}{2}$	2.22	57.0	388	8800	35.6	98.7	4.30	3.11	184
$1\frac{3}{4}$	2.41	68.3	361	7900	32.4	107	5.10	4.30	247
1.9	2.51	74.3	348	7600	31.2	112	5.42	5.10	296
2	2.58	78.3	338	7300	30.0	115	5.58	5.64	330
$2\frac{1}{4}$	2.75	89.0	320	6810	28.2	122	6.06	7.10	399
$2\frac{1}{2}$	2.91	99.6	305	6320	26.4	129	6.29	8.65	450
$2\frac{3}{4}$	3.05	109.5	291	6040	25.2	135	6.48	10.3	498
3	3.20	121	280	5640	23.8	142	6.59	11.9	545
$3\frac{1}{4}$	3.34	132	268	5350	22.5	147	6.42	13.5	594
$3\frac{1}{2}$	3.46	141	259	5150	21.8	153	6.28	15.1	641
$3\frac{3}{4}$	3.60	153	251	4850	20.6	158	6.15	16.7	660
4	3.72	163	243	4700	20.0	163	6.06	18.2	656
$4\frac{1}{2}$	3.96	184	230	4410	18.9	173	6.24	21.2	643
5	4.17	204	219	4070	17.5	182	6.40	24.4	633
$5\frac{1}{2}$	4.39	227	208	3870	16.7	190	6.70	27.6	633
6	4.60	249	200	3720	16.1	198	7.00	31.2	638
$6\frac{1}{2}$	4.79	270	193	3530	15.4	206	6.83	34.6	637
7	4.98	292	186	3380	14.8	214	6.55	38.0	634
$7\frac{1}{2}$	5.17	315	180	3280	14.4	221	6.42	41.2	637
8	5.34	336	174	3080	13.5	228	6.52	44.5	629

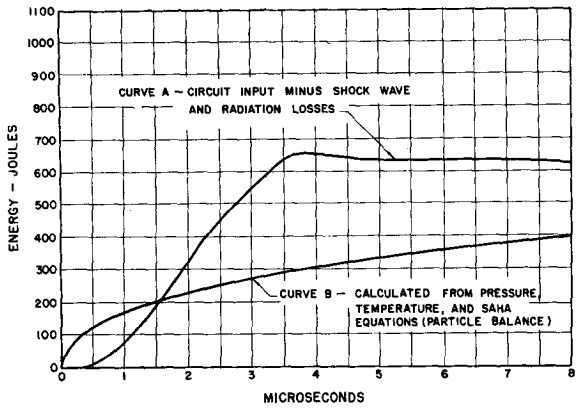

FIG. 6. Energy stored in the 25-kv underwater spark channel. Summary of results of the entire energy balance.

involving Saha ionization equations and dissociation equations, will be a nonlinear set, and hence, explicit solutions will be inconveniently complicated as far as algebraic manipulation is concerned. In the present study, this complication in obtaining the particle balance solution was avoided by assuming initially that certain particle types were present in negligible amounts in the plasma, and hence, the appropriate terms in the equations could be neglected. The resulting particle balance solutions then supplied information which could be used to confirm that the original assumptions were in fact correct.

The types of particles which could conceivably be found in the underwater spark plasma are water molecules, oxygen molecules, hydrogen molecules, ozone molecules, oxygen atoms in all degrees of excitation and ionization, hydrogen atoms in all degrees of excitation (and singly ionized), tungsten atoms in all levels of excitation and ionization, copper atoms (from the electrodes) in all levels of excitation and ionization, hydroxyl (OH) groups, and negative hydrogen ions formed by electron attachment. This list could be made more extensive by adding such molecules as copper oxide and by considering that all molecule types may themselves be excited or ionized.

Copper will be eliminated from consideration, since there is not sufficient time for copper to migrate from the electrode regions into the spark. The kinetic theory calculated mobility for copper (an upper limit to the true value) is 2.4×10^{-6} m^2/sec v, and the typical electrical gradient is 3.3×10^5 v/meter. This gives a migration distance of only 2×10^{-5} m in 24 μsec. This is small compared to the spark length of 1.5×10^{-2} m. Tungsten may also be eliminated from consideration. It will be shown later that the tungsten atoms are multiply ionized, but since there are so few of them present compared to the total particle density, they store a negligible amount of energy and contribute a negligible number of free electrons to the plasma. Subsequent analysis will also show that there is a negligible amount of second ionization of the oxygen atoms, so that only neutral and singly ionized oxygen need be considered. Ozone, hydroxyl groups, and negative hydrogen ions will be considered to exist in negligible numbers, since they are either unstable at high temperatures or have small dissociation energies.

The degrees of dissociation of water, oxygen, and hydrogen molecules were investigated using the dissociation relation of Gibson and Heitler.[6] This relation strictly applies only to diatomic molecules, but was also applied to the triatomic water molecule by choosing the moment of inertia and characteristic frequency to obtain the minimum degree of dissociation. It was found that undissociated water constitutes at most less than 1% of the total number of particles present in the plasma. As applied to oxygen molecules, the dissociation relation showed that there are less than 3% as many oxygen molecules as there are oxygen atoms present. The fraction of hydrogen molecules was similarly found to be much less than 3% of the number of hydrogen atoms present. The conclusion was therefore reached that undissociated molecules constitute at most only several percent of the total number of plasma particles and may therefore be neglected.

The remaining numerically important particle types were determined by solving the following simultaneous particle-balance equations:

$$N_{\mathrm{HI}}+N_{\mathrm{HII}}+N_{\mathrm{OI}}+N_{\mathrm{OII}}+N_e=N, \tag{5}$$

$$N_{\mathrm{HI}}+N_{\mathrm{HII}}=2N_{\mathrm{OI}}+2N_{\mathrm{OII}}, \tag{6}$$

$$N_{\mathrm{HII}}+N_{\mathrm{OII}}=N_e, \tag{7}$$

$$N_{\mathrm{HII}}N_e=N_{\mathrm{HI}}S_{\mathrm{H}}, \tag{8}$$

$$N_{\mathrm{OII}}N_e=N_{\mathrm{OI}}S_{\mathrm{O}}, \tag{9}$$

where N is the total particle density, N_e is the electron density, N_{HI} is the hydrogen atom density, N_{HII} is the hydrogen ion density, S_{H} is the Saha factor for hydrogen, and O subscripts designate similar terms for oxygen. These equations were supplemented by a large number of Boltzmann excitation relations. Since each Boltzmann relation introduced one unknown term as well as supplying one equation, the excitation relations were subsequently introduced after the above particle balance equations were solved. The Saha factor is given by

$$S=\frac{2B'(T)}{B(T)}\left(\frac{2\pi m_e k}{\mathrm{h}^2}\right)^{\frac{3}{2}}T^{\frac{3}{2}}\exp\left(\frac{-11\,600V}{T}\right), \tag{10}$$

where $B(T)$ is the atom partition function, $B'(T)$ is the ion partition function, m_e is the electron mass, and V is the ionization potential in volts. Other terms have the usual meanings.

The particle balance equations were completely solved for three selected instants of time during the spark cycle: one-half μsec, 1.9 μsec (current maximum), and 4 μsec (first current zero). The value of N was ob-

[6] G. E. Gibson and W. Heitler, Z. Physik **49**, 465 (1928).

tained by employing the ideal gas law as the equation of state of the plasma. Subsequently, it will be concluded that the plasma has an internal pressure caused by interparticle Coulomb fields, and hence the N obtained is only an approximation. The pressure term in the ideal gas law included not only the calculated external pressure (7600 atmos at 1.9 μsec) but also the average pinch pressure (735 atmos at 1.9 μsec). The partition functions, which are nonconvergent infinite series, were evaluated by a simplified form of the method of excluded volumes of Urey and Fermi.[7] This concept of excluded volumes also leads to appropriately reduced ionization potentials. The solutions to the particle balance equations at current maximum, including the excitation as obtained from the Boltzmann relations, are presented in Table III. To each particle type in this table there may be ascribed a certain amount of energy. This in general consists of water vaporization energy, dissociation energy, excitation energy, ionization energy (based on reduced ionization potentials), and kinetic energy of thermal motion. The ionization energies have been associated with the product ions, leaving only the kinetic energy of random motion to be ascribed to the resultant electrons. This obviated subdividing the electrons into groups according to their origin, and therefore simplified the calculations. The appropriate energies per particle at current maximum are given in column 3 of Table III. The resulting energy densities per particle type are given in column 4. Summation of column 4 gives the energy density in the plasma at current maximum, 3.08×10^9 joules/meter^3. A similar procedure carried out at $\frac{1}{2}$ and at 4 μsec yielded stored energies of 7.0×10^9 and 1.8×10^9 joules/meter^3 respectively. Calculations showed that a negligible amount of energy was stored by induced polarization of the hydrogen atoms and the oxygen atoms and ions.

TABLE III. Particle balance at 1.9 μsec (current maximum, 85 000 amp).

Particle type	Particle density (per cubic meter) ($\times10^{26}$)	Energy per particle (ev)	Energy density (joules per cubic meter) ($\times10^8$)
Neutral hydrogen			
ground state	6.75	7.2	7.78
first excited state	0.52	17.4	1.45
Ionized hydrogen	3.01	17.7	8.55
Neutral oxygen			
ground state	2.48	7.2	2.86
first excited state	0.645	9.2	0.950
second excited state	0.055	11.4	0.101
third excited state	0.061	16.5	0.162
Ionized oxygen			
ground state	0.977	17.7	2.77
first excited state	0.675	21.0	2.27
second excited state	0.210	22.7	0.764
third excited state	0.0092	32.6	0.048
fourth excited state	0.0042	40.8	0.027
Electrons	4.48	3.9	3.05
Total	2.02×10^{27}		3.08×10^9

TABLE IV. Stored energy density in water (excitation energy neglected).

Pressure atmos	Temperature (°K)	Energy density (joules per cubic meter)
4 150	31 500	1.45×10^9
8 300	31 500	2.80×10^9
20 000	31 500	6.38×10^9
8 300	40 000	2.73×10^9
8 300	60 000	2.62×10^9
8 300	200 000	2.78×10^9

Highly ionized tungsten from the initiating wire contributes an additional 0.72×10^9 joules per cubic meter at 200 000°K.

The known volume of the tungsten initiating wire, together with simultaneous Saha equations, allowed the number densities of tungsten atoms in various stages of ionization to be determined. Appropriately reduced ionization potentials were used. The results showed that at current maximum in the underwater spark, most of the tungsten was singly and doubly ionized, the populations of these two levels being about equal. The consequent density of stored energy was found to be $\frac{1}{2}$% of the energy density stored by dissociation, excitation, and ionization of water. The tungsten also contributed a negligible number of particles to the channel in comparison with those furnished by the water. Similarly, the amount of second ionization of oxygen may be determined. The results showed that there was about 0.05% as many doubly ionized oxygen ions as singly ionized ions, so that the resultant energy storage was negligible.

An interesting result of the calculations of energy density may be obtained by taking the ratio of energy density to channel pressure (including average pinch pressure) and plotting the result as a function of time. The ratio is found to be constant to an accuracy of about 12%. This proportionality of energy density to pressure was investigated further by applying the particle balance equations to the products of dissociation of water over a more extended pressure and temperature range than is encountered in the underwater spark. The results, which neglect energy of excitation, are summarized in Table IV. Over the range of pressures and temperatures calculated, the energy density is approximately proportional to pressure and almost independent of temperature. By making use of this constant ratio between energy density and pressure, and employing the volume of the spark as obtained from the Kerr cell photographs, one may plot a curve of total energy stored in the underwater spark as a function of time. The result is shown as Curve B in Fig. 6. This curve constitutes the second part of the energy balance. Agreement between Curves A and B would indicate complete accounting for all of the energy in the spark channel at any instant of time.

[7] R. H. Fowler, *Statistical Mechanics* (Cambridge University Press, Cambridge, 1936), second edition.

DISCREPANCIES IN THE ENERGY BALANCE

The differences between Curves A and B may be qualitatively and semiquantitatively resolved. The fact that Curve A goes slightly negative reveals that the calculated external pressures were somewhat too large, which indicates that the actual rate of channel growth was less than that used in the calculations. The method of determining the rate of channel growth introduces some uncertainty, but a major factor is the effect of optical magnification as a result of the pressure gradient adjacent to the spark channel surface. The shock wave calculations lead to a pressure gradient of 5.8×10^7 atmos/m at $\frac{1}{2}$ μsec and 2.15×10^7 atmos/m at 1 μsec. These pressure gradients were converted to refractive index (n) gradients by assuming $n-1$ to be proportional to mass density. Appreciable curvature of a light ray results, and the consequent effect on the apparent channel size was approximately determined graphically by ray tracing. The amount of magnification at $\frac{1}{2}$ and 1 μsec was of the order of 15%. The consequent change in the channel growth curve tends to raise Curve A, since the calculated mechanical work output and radiated energy are both reduced. It also tends to lower Curve B, since the lower pressure leads to a lower energy density which, in conjunction with the smaller spark volume, gives a lower channel energy. After the first μsec or so the preceding effects become unimportant, since the larger channel diameter and the lower pressure gradient yield less channel magnification.

The differences between Curves A and B at times substantially later than 1.6 μsec are probably caused by inaccuracy of Curve B due to the use of the ideal gas law as the equation of state of the plasma. The particle density within the plasma is of the order of $\frac{1}{10}$ of that found in solids or liquids, and the degree of ionization is approximately 30%. Under such conditions the plasma cannot be expected to behave as an ideal gas. The deviation from ideal behavior may be obtained by calculating the internal pressure which is produced by the interparticle Coulomb fields.

The general pressure relations for any gas are included in the equation,

$$P_{\text{external}}+P_{\text{pinch}}+P_{\text{attraction}}=P_{\text{kinetic}}+P_{\text{repulsion}}, \quad (11)$$

where P_{external} is the calculated pressure which generates the shock wave, P_{pinch} is the average pinch pressure, $P_{\text{attraction}}$ and $P_{\text{repulsion}}$ are the components of pressure ascribable to attractive and repulsive forces between particles, and P_{kinetic} is the component of pressure (NkT) resulting from kinetic motion of the particles. The separation of the attraction and repulsion pressures is somewhat artificial; the two are usually combined and calculated from the interparticle force law in the form of the second virial coefficient. The resulting pressure may be placed on the left side of Eq. 11 as $P_{\text{attraction}}-P_{\text{repulsion}}$. It is then referred to as the internal pressure. Knowledge of the external, pinch, and internal pressures thus enables one to compute the kinetic pressure and, therefore, the true particle density.

There are two basic reasons why the conventional integral expressions for the internal pressure cannot be applied to the present case involving a highly ionized gas. The first of these is concerned with the long-range nature of the Coulomb force law. The integrals involved are derived on the assumption of binary collisions only. Closely related to this is the fact that the integrals are nonconvergent for interparticle force laws which decrease less rapidly than the inverse fourth power of the particle separation. For an inverse-square law of force, the motion of a particle is appreciably affected by particles well beyond the nearest neighbors. This suggests that the concepts of mean free path and binary collisions have no place in the analysis of highly ionized gases. The second basic reason why the usual integral forms for the internal pressure cannot be used is that they are based on the assumption of identical force laws between all particle types. For a highly ionized gas there are repulsion forces between some pairs of particles, attraction forces between other pairs, and negligibly small forces (due to polarization and short-range interactions) between other pairs. As a result, another approach must be used to evaluate the internal pressure in a highly ionized plasma. The approach used here is based on the concept of the Debye shielding distance. If the particle densities already calculated are used, the Debye length is found to be about 4 A for the plasma of the underwater spark. This length gives the order of magnitude of the distance beyond which only collective particle motions exert an appreciable effect on the motion of a given particle. However, for the same conditions, the average particle separation is found to be about 10 A. These results suggest that the entire plasma surrounding a given particle may be treated as a polarizable continuum; i.e., individual interactions of a given particle with its nearest neighbors may be neglected.

Consider a sphere surrounding any particular plasma ion (Fig. 7). Choose the radius of the sphere so that its volume is the average volume per particle of the plasma. Polarization of the plasma by the ion may be represented by a surface charge density uniformly distributed over the surface of the sphere. If one computes the forces between the central ion and the enclosing spherical charge shell (allowing for mutual repulsion between the

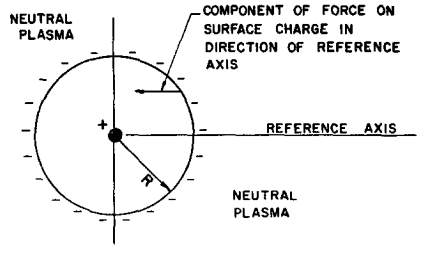

FIG. 7. Calculation of internal pressure within the plasma.

charges on the shell), one finds there is a net force holding any two hemispheres of the outer shell together. This net force divided by the cross-sectional area of the sphere is a measure of the internal pressure caused by the interparticle Coulomb forces. The result is

$$P_{\text{internal}}=\frac{q^2}{32\pi^2\epsilon_0 R^4} \tag{12}$$

where q is the charge on the ion, R is the radius of the enclosing sphere (meters), and ϵ_0 is the dielectric constant of free space (MKS rationalized units). This equation may be solved simultaneously with Eq. (11) for the particle density N in terms of external and pinch pressures and temperature. When applied to the conditions in the underwater spark at current maximum, this procedure yields a total particle density of 2.5×10^{27} particles/meter^3, and an internal pressure of 2170 atmos. This result has significance in that it indicates that the internal pressures are of the same order of magnitude as the external pressures, and hence should not be neglected. The new value of N thus obtained may be used as the basis of a revised particle balance. It would be found that a greater amount of energy would be stored in the spark channel than is indicated by Curve B of Fig. 6. This would serve to bring the two energy balance curves into better agreement. The discrepancy between Curves A and B at times later than 1.6 μsec may conceivably be treated as an experimental measure of the magnitude of the internal pressure within the plasma.

ADDITIONAL CONCLUSIONS BASED ON THE PARTICLE BALANCE

The particle densities obtained from the energy balance calculations may be utilized to obtain additional information about the underwater spark plasma. If the amount of water in the channel (based on the particle balance) is plotted *vs* time, one may obtain the rate of induction of water through the spark channel wall. At current maximum, this is found to be 10^{25} molecules/sec, requiring an inducting power of 55 megawatts. It should be noted that this power does not leave the channel. It is improbable that this amount of power is transferred to the channel wall from the core by thermal conduction. The thermal conductivity of the plasma, soon to be computed, is sufficiently low so that a central temperature on the spark axis of several million degrees would be required. Temperatures of this order are not to be expected in view of the insensitivity of the major spark parameters to changes in surface to volume ratio as mentioned earlier. If the surface recombination rate is computed, however, and one assumes that all ions impinging on the channel wall do recombine, then an energy of 348 megawatts is available. Therefore, only one-eighth of the ions striking the wall need recombine in order to furnish the necessary induction energy. The rate of induction of water molecules also allows one to determine the rate of radial expansion of the channel wall caused by water induction. The result at current maximum is 10 m/sec, which is not large enough to invalidate the hydrodynamic pressure calculation described earlier.

The electrical conductivity of the plasma should not be computed on the basis of the usual kinetic theory concept of a mean free path because of the importance of the Coulomb interparticle fields. Gvosdover has developed an expression for the effective collision cross section for electrons moving through positive ions.[8] If the Gvosdover cross section is used in computing the electrical conductivity of the underwater spark plasma at current maximum, the result is 5.4×10^4 mhos/m. Spitzer and Harm have developed a theory for the electrical conductivity of a completely ionized plasma.[9] Their theory applied to the underwater spark plasma at current maximum yields an electrical conductivity of 10×10^4 mhos/m. Both of these computed conductivities are in good agreement with the value experimentally obseved in this study. The experimental conductivity at current maximum is 5.6×10^4 mhos/m.

The theory of Spitzer and Harm yields a thermal conductivity for the underwater spark plasma at current maximum of 86 w/m °K. This theory is based on the kinetic motion of the plasma particles only, and neglects contributions to the thermal conductivity caused by radiation exchange and gradients of dissociation, excitation, and ionization. Preliminary order-of-magnitude calculations indicate that these latter mechanisms do not contribute significantly to the thermal conductivity of the underwater spark plasma.

The channel wall of the underwater spark is a complex region. The temperature gradient is very large so that thermodynamic equilibrium cannot be expected to exist among the particles. The differing coefficients of diffusion of electrons and ions in the plasma establish a large electrical gradient across the wall. The magnetic field in this region is about 13.5 webers/m^2 (135 000 gauss) at current maximum. Also, the degrees of dissociation, excitation, and ionization change rapidly across this region. Finally, the channel wall is probably not a gas-to-liquid interface because the pressures are very much higher than the critical pressure of water. The channel wall may therefore be considered to be a transition region of small but finite thickness where all physical characteristics vary continuously from cool liquid water to highly ionized plasma.

ACKNOWLEDGMENTS

The author is indebted to W. G. Dow and H. C. Early for their many helpful discussions. The work was supported in part by the U. S. Army Office of Ordnance Research.

[8] H. Maecker, Ergeb. exakt. Naturw. **25**, 310 (1951).
[9] L. Spitzer and R. Harm, Phys. Rev. **89**, 977 (1953).